Effective Mass Anisotropy of Γ Electrons in GaAs/AlGaAs Quantum Wells

T. Reker, H. Im,* L. E. Bremme, H. Choi, Y. Chung, and P. C. Klipstein

Clarendon Laboratory, Department of Physics, University of Oxford, Parks Road, Oxford, OX1 3PU, United Kingdom

Hadas Shtrikman

Braun Center for Submicron Research, Weizmann Institute of Science, Rehovot 76100, Israel

Resonant magnetotunneling in GaAs/Al$_{0.28}$Ga$_{0.72}$As double barrier structures is used to demonstrate that the effective mass of confined Γ conduction electrons becomes anisotropic when an electric field is applied perpendicular to the interfaces. Although several authors have previously reported Γ-related optical anisotropy, this is the first example of a corresponding *electrical* anisotropy. The results are explained using a quantum mechanical model involving interface band mixing that contains additional features not found in the optical case.

In the past few years, it has become evident that the interfaces in semiconductor heterostructures can play a subtle but highly significant role which goes beyond the obvious one of phonon or electron confinement [1−4]. For example, anisotropy has recently been reported in the polarization of light along the two in-plane ⟨110⟩ directions for optical transitions in quantum wells (QWs) [5−8]. It has been proposed that such behavior arises from the interface induced mixing between zone center Γ$_{15x}$ and Γ$_{15y}$ valence states [9].

Recently, some of the authors have reported very strong *electrical* anisotropy in AlAs QWs, where the in-plane effective mass of X electrons is different for the two ⟨110⟩ directions. This electrical anisotropy is caused by interface band mixing of zone boundary X_X and X_Y electrons, and can thus also be characterized by an "x-y" mixing mechanism [10]. To our knowledge there has been no report of a similar electrical anisotropy for Γ electrons. Such anisotropy is to be expected since all of the above optical and mass anisotropies should relate to the orthogonal ⟨110⟩ orientations of bond planes at opposite interfaces of the QW (Fig. 1). Anisotropy will occur when the equivalence of the two ⟨110⟩ directions is destroyed, e.g., by the application of an electric field along [001]. In this Letter we present the first observation of effective mass anisotropy for Γ$_1$ electrons. However, unlike in the previous cases of optical anisotropy, we show that two mixing contributions are required: Γ$_{15x}$ with Γ$_{15y}$ states ("x-y" mixing) and Γ$_1$ with Γ$_{15z}$ states ("Γ-z" mixing).

Resonant magnetotunneling spectroscopy ($B \perp J$) has been used widely in double barrier structures (DBSs), to probe the in-plane dispersions of QW states [10–12]. We apply this technique here to sample the in-plane dispersion anisotropy of two symmetric DBSs grown by molecular-beam epitaxy along [001], consisting of 80 Å spacers, 80 Å Al$_{0.28}$Ga$_{0.72}$As barriers, and a 120 Å wide GaAs QW. The emitter and collector regions, including spacers, were Al$_x$Ga$_{1-x}$As with $x \sim 0.05$ and 0.06, respectively. Silicon doping of 2×10^{17} cm^{-3} was present in the emit-

ter and collector. $I(V)$ measurements were performed at $T = 1.5$ K.

Figure 2(a) shows the $I(V)$ characteristics of the $x = 0.05$ sample as a function of magnetic field up to $B = 10$ T, applied parallel to a ⟨100⟩ direction. Note the high degree of symmetry between bias directions. The Γ(2) resonant tunneling peaks, at approximately ±0.2 V, are easily discernible and they shift to higher bias, and also broaden, with increasing magnetic field. In Fig. 2(b), the peak positions are plotted against B^2. According to the semiclassical interpretation of resonant magnetotunneling [12,13], the peak bias shift should be proportional to the dispersion energy of the confined state in the well, at a wave vector whose magnitude and direction are proportional and perpendicular, respectively, to those of the magnetic field [10,12]. Deviations from this behavior are known to occur at small magnetic fields [11,14]. For $B \geq 5$ T, the measured data in Fig. 2(b) exhibit a parabolic
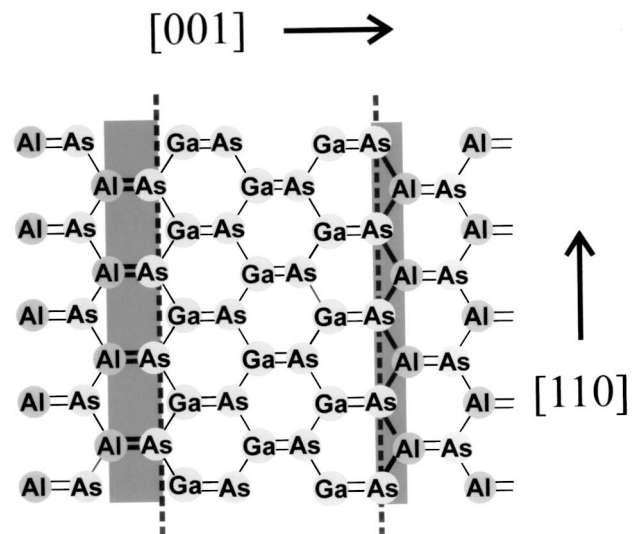

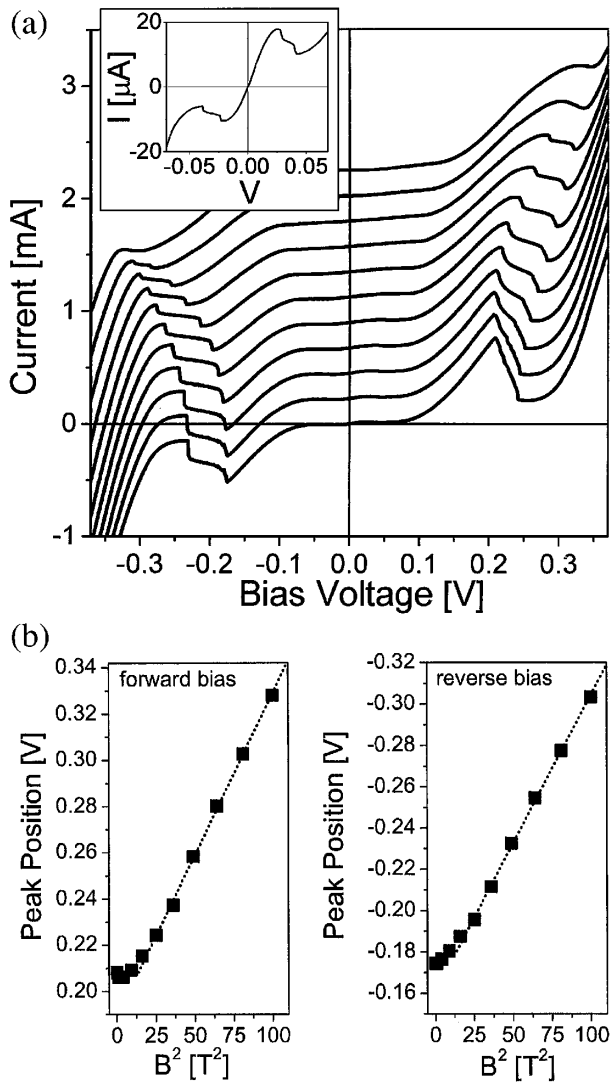FIG. 1. The bonding arrangement in an AlAs-GaAs-AlAs quantum well.

FIG. 2. (a) $I(V)$ characteristics (100 μm mesa) showing the $\Gamma(2)$ resonances in the $x = 0.05$ sample as a function of magnetic field along a $\langle 100 \rangle$ direction between $B = 0$ T (bottom) and 10 T (offset for clarity). Inset: the $\Gamma(1)$ resonances. (b) $\Gamma(2)$ peak position plotted against B^2—the dotted lines show a linear fit to the data for $B \geq 5$ T.
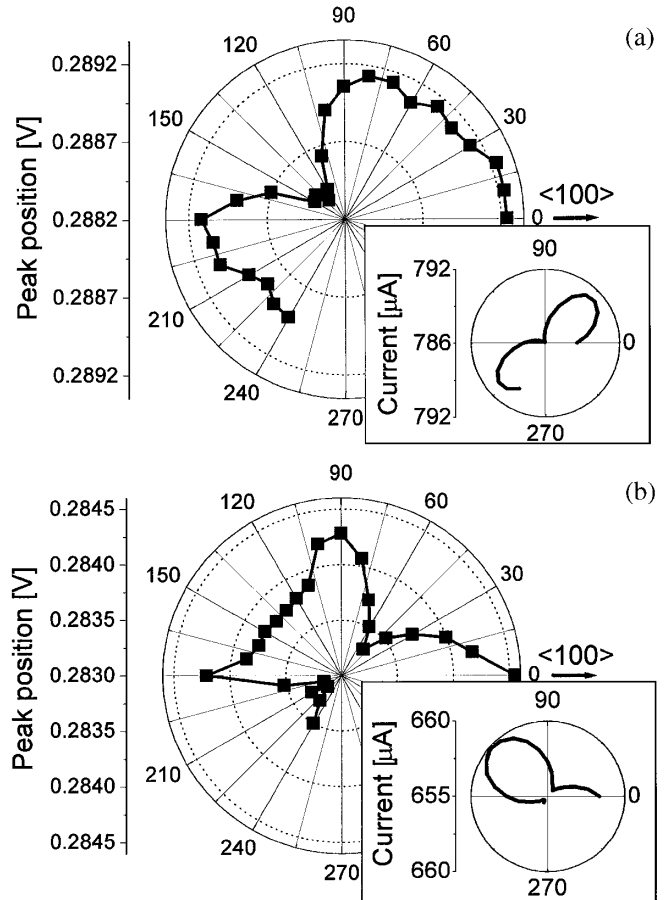

FIG. 3. Dependence of the peak bias position on the in-plane magnetic field direction for the $\Gamma(2)$ resonance in the $x = 0.05$ sample. Magnetic fields of 8.4 and 9.25 T were applied in (a) the forward and (b) the reverse bias directions, respectively. Insets: peak current vs magnetic field direction.

field dependence, consistent with the parabolic dispersion relation for electrons in the well. In this region, the shift of the peak position from a bias value found by extrapolating back the parabolic dependence to $B = 0$ is thus a true measure of the dispersion energy.

To within the resolution (≈ 100 μeV) of our setup, the bias position of the $\Gamma(1)$ resonance [inset of Fig. 2(a)] was isotropic with respect to the angle of the in-plane magnetic field. Figure 3 shows the angle dependence of the $\Gamma(2)$ peak position. The field was aligned initially along a $\langle 100 \rangle$ direction. Subsequent $I(V)$ characteristics were measured every 10° up to 240° from this position. Figure 3 reveals a twofold anisotropy in both forward and reverse bias. The main axes of the anisotropy are oriented along the two orthogonal $\langle 110 \rangle$ directions, with a clear 90° rotation

between forward and reverse bias. This shows that the constant energy surface of the $\Gamma(2)$ subband is *anisotropic,* with its principal axes oriented along the $\langle 110 \rangle$ directions and that the constant energy surface rotates by 90° on changing the bias polarity. Further, we find that the peak current shows the same anisotropy and 90° rotation (insets of Fig. 3).

Figure 4 shows a plot of the peak position vs magnetic field direction for the forward bias $\Gamma(3)$ resonance in the $x = 0.06$ sample at $B = 5$ T. For $B \geq 4$ T, this resonance shifts to higher bias linearly in B^2, as shown in the inset. Figure 4 shows similar behavior to that seen for the $\Gamma(2)$ resonance in Fig. 3(a). We obtain a mass difference between the [110] and [$\bar{1}$10] directions of $\sim 1\%$ for the $\Gamma(2)$ resonance and $\sim 3\%$ for the $\Gamma(3)$ resonance. The $\Gamma(1)$ resonance in both samples showed no bias shift but only a small current anisotropy (similar to the insets of Fig. 3), indicating that weak anisotropy exists even for the $\Gamma(1)$ resonance. From the behavior of all three resonances, we conclude that the size of the effective mass anisotropy increases with electric field.
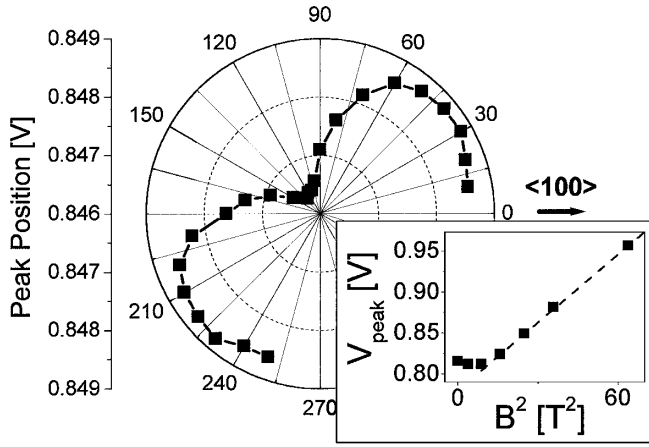
FIG. 4. Behavior of the $\Gamma(3)$ resonance in the forward biased $x = 0.06$ sample. Inset: peak bias vs B^2 for $B \parallel \langle 100 \rangle$. The dotted line shows a linear fit to the data for $B \geq 4$ T.

In the remainder of this Letter, we present a simple quantum mechanical model to explain our results. In a typical GaAs/AlAs QW or superlattice, the bonding Γ_{15v} (antibonding Γ_{15c}) profile has a type-I (type-II) alignment ~ 1.5 eV below (~ 1 eV above) the Γ_{1c} conduction band. In such a structure, the planes containing the Ga-As and As-Al *interfacial* bonds are orthogonal and oriented along the [110] and [$\bar{1}$10] directions, denoted x' and y', respectively. If we define a virtual crystal, whose microscopic potential is the average of those for GaAs and AlAs, the Ga and Al atoms will acquire equal and opposite charges $\pm \delta q$, relative to the virtual crystal. We can also define a microscopic interface potential, V_{INT}, which extends $\pm a_0/4$ in the z direction from the interface plane of As atoms at z_i (a_0 is the cubic lattice parameter), and which, when added to the potential of the virtual crystal, yields that of the actual crystal in that region [15,16]. The tetrahedral bonding of the atoms then leads to the relation $V_{INT}(x', y', z - z_i) = -V_{INT}(y', x', -z + z_i)$. From this it follows that $\langle X'|V_{INT}|X'\rangle = \alpha$, $\langle Y'|V_{INT}|Y'\rangle = -\alpha$, and $\langle \Gamma_1|V_{INT}|Z\rangle = -i\beta$, where $|X'\rangle$ is a crystal periodic function (CPF) of the virtual crystal with its p orbital oriented along x' (analogous definitions apply to $|Y'\rangle$ and $|Z\rangle$), where α, β are real constants, and where $|\Gamma_1\rangle = |iS\rangle$ is a CPF based on antibonding s orbitals. Throughout this discussion, we use the CPF basis of Ref. [17] for the virtual crystal. We consider only the spin up Γ_1 state, since the analogous treatment for the spin down case is obvious. With a simple transformation of coordinates, it is found that

$$
\begin{aligned}
\langle X|V_{INT}|X\rangle = \langle Y|V_{INT}|Y\rangle &= \langle Z|V_{INT}|Z\rangle \\
&= \langle \Gamma_1|V_{INT}|\Gamma_1\rangle = 0, \\
\langle X|V_{INT}|Y\rangle = \langle Y|V_{INT}|X\rangle &= \alpha, \\
\langle \Gamma_1|V_{INT}|Z\rangle &= -i\beta.
\end{aligned}
\tag{1}
$$

It has been shown in Refs. [15,16] that matrix elements which contain V_{INT} and the relevant CPFs, such as those derived in Eq. (1), can lead to δ-function–like interface band mixing.

We will now show that both mixing potentials, α and β, contribute to the observed mass anisotropy, unlike in the optical case discussed later, where only α contributes [5,7]. Here, we use standard $\boldsymbol{k} \cdot \boldsymbol{p}$ theory [17], in which the mixing between Γ_1 and any one of the Γ_{15} states, denoted $\Gamma_{15\sigma}$, has the matrix element: $H_{\boldsymbol{k}\cdot\boldsymbol{p}}^{\Gamma_1,\sigma} = -\sum_{x_i=x,y,z} \frac{\hbar^2}{m_0} \langle u_{\Gamma_1}| \frac{d}{dx_i} |u_{\Gamma_{15\sigma}}\rangle \frac{d}{dx_i}$. For example, if $u_{\Gamma_{15\sigma}}$ represents the CPF $|j, m_j\rangle = |3/2, 3/2\rangle$, then $H_{\boldsymbol{k}\cdot\boldsymbol{p}}^{\Gamma_1,\sigma} = i\frac{P_0}{\sqrt{2}}(\frac{\partial}{\partial x} + i\frac{\partial}{\partial y})$, where P_0 is a real constant. For particular Γ_1 and Γ_{15} states, $|\nu\rangle$ and $|\sigma\rangle$, with envelope functions $\Psi_{\Gamma_1}^{\nu} = e^{ik_x x} e^{ik_y y} \phi(z)$ and $\Psi_{\Gamma_{15}}^{\sigma} = e^{ik_x x} e^{ik_y y} \theta(z)$, respectively, this gives a matrix element: $\langle \nu|H_{\boldsymbol{k}\cdot\boldsymbol{p}}^{\Gamma_1,\sigma}|\sigma\rangle = -\frac{P_0}{\sqrt{2}}(k_x + ik_y)\langle\phi | \theta\rangle$, which is finite only when ϕ and θ have the same parity. The wave functions of the confined states, $E(n)$, in the QW conduction band, thus have the form

$$
\begin{aligned}
|\Gamma(n)\rangle = \{&\phi_n(z)|\Gamma_1\rangle + \theta_n(z)(k_x + ik_y)|X + iY\rangle \\
&+ \vartheta_n(z)(k_x - ik_y)|X - iY\rangle \\
&+ \Psi_n(z)|Z\rangle\} e^{i\boldsymbol{k}_\parallel \cdot \boldsymbol{\rho}},
\end{aligned}
\tag{2}
$$

where the second term contains contributions from the Γ_{15v} or Γ_{15c} CPFs $|3/2, 3/2\rangle$, the third from $|3/2, -1/2\rangle$ and $|1/2, -1/2\rangle$, and the fourth from $|3/2, 1/2\rangle$ and $|1/2, 1/2\rangle$. In Eq. (2), $\boldsymbol{\rho}$ and $\boldsymbol{k}_\parallel$ are the in-plane position and wave vectors, respectively. Rearranging, we have

$$
\begin{aligned}
|\Gamma(n)\rangle = \{&\phi_n(z)|\Gamma_1\rangle + [\Xi_n(z)k_x + i\Theta_n(z)k_y]|X\rangle \\
&- [\Xi_n(z)k_y - i\Theta_n(z)k_x]|Y\rangle \\
&+ \Psi_n(z)|Z\rangle\} e^{i\boldsymbol{k}_\parallel \cdot \boldsymbol{\rho}},
\end{aligned}
\tag{3}
$$

where $\Xi_n(z) = \theta_n(z) + \vartheta_n(z)$ and $\Theta_n(z) = \theta_n(z) - \vartheta_n(z)$. In Eq. (3), all the envelope functions are real except the Ψ_n, which are purely imaginary. The parities with respect to the center of the GaAs layer are given in Table I.

Limiting ourselves to the basis $\{|\Gamma(1)\rangle, |\Gamma(2)\rangle\}$, we can now illustrate the changes caused by the interface band mixing. The conduction band is then described by a simple 2×2 Hamiltonian with diagonal elements, E_1 and E_2, and off-diagonal elements, $V_{12}(k_x, k_y)$ and $V_{12}^{\dagger}(k_x, k_y)$, in

TABLE I. Parity properties of the envelope functions for the $|\Gamma(1)\rangle$ and $|\Gamma(2)\rangle$ states.

Even				Odd			
$\phi_1(z)$	$\Xi_1(z)$	$\Theta_1(z)$	$\Psi_2(z)$	$\phi_2(z)$	$\Xi_2(z)$	$\Theta_2(z)$	$\Psi_1(z)$

which

$$V_{12}(k_x, k_y) = \langle \Gamma(1) | V_{\text{INT}} | \Gamma(2) \rangle$$

$$= \sum_i \alpha P_i \{ [\Theta_1^*(z_i)\Theta_2(z_i) - \Xi_1^*(z_i)\Xi_2(z_i)] 2k_x k_y + i[\Xi_1^*(z_i)\Theta_2(z_i) - \Theta_1^*(z_i)\Xi_2(z_i)](k_x^2 - k_y^2) \}$$

$$- i\beta P_i [\phi_1^*(z_i)\Psi_2(z_i) + \phi_2(z_i)\Psi_1^*(z_i)]$$

$$= A_{12} k_x k_y + i B_{12}(k_x^2 - k_y^2) + C_{12}, \qquad (4)$$

where the summation is over both QW interfaces and $P_i = 1$ (-1) for a normal (inverted) interface. Here, A_{12}, B_{12}, and C_{12} are real. In zero electric field, $A_{12}, B_{12} \neq 0$, but $C_{12} = 0$, so the dispersions in the two $\langle 110 \rangle$ directions are identical. However, in a nonzero electric field all three coefficients become finite, so that if the contributions from A_{12} and C_{12} add for the [110] direction, they will cancel for the [$\bar{1}10$] direction, and vice versa. This leads to anisotropy in the constant energy surface, so that the effective masses along [110] and [$\bar{1}10$] are no longer the same. It is also clear from Eq. (4) that, on reversing the electric field, the sign of C_{12} changes, thereby interchanging the dispersions for [110] and [$\bar{1}10$] and rotating the constant energy surface of each subband by 90°. The interchange and rotation still occur if more basis states are included. This follows from the fact that for a given pair of subbands, i and j, either A_{ij} or C_{ij} change sign with a reversal in the electric field, but not both at the same time.

The preceding model, based on x-y and Γ-z mixing, explains well the key features of our measurements, namely, the existence of a mass anisotropy that increases with perpendicular electric field, and that rotates by 90° when the field is reversed. We also note that x-y mixing as in Eq. (1) leads to mixing between heavy and light holes [9]. Using a basis of the first confined heavy-hole and the first two confined light-hole states, we obtain excellent agreement with the optical anisotropy measurements of Kwok *et al.* [5] if $\alpha \approx 0.5$ eV Å, a value consistent with Ref. [16].

In conclusion, we have observed a small $\langle 110 \rangle$ effective mass anisotropy for Γ electrons in GaAs/AlGaAs QWs. The anisotropy is caused by interference between contributions from x-y and Γ-z interface band mixing. Our results contrast with the large mass anisotropy observed for X electrons, recently related to interference between two different x-y contributions, having X_1 and X_3 symmetry. Interference between two contributions thus appears to be a common characteristic of mass anisotropy in QWs.

*Presently at Department of Semiconductor Science, Dongguk University, Seoul, Korea.

[1] A. K. Sood, J. Menendez, M. Cardona, and K. Ploog, Phys. Rev. Lett. **54**, 2115 (1985).

[2] I. Sela, L. A. Samoska, C. R. Bolognesi, A. C. Gossard, and H. Kroemer, Phys. Rev. B **46**, 7200 (1992).

[3] S. G. Lyapin, P. C. Klipstein, N. J. Mason, and P. J. Walker, Phys. Rev. Lett. **74**, 3285 (1995).

[4] P. V. Santos, P. Etchegoin, M. Cardona, B. Brar, and H. Kroemer, Phys. Rev. B **50**, 8746 (1994).

[5] S. H. Kwok, H. T. Grahn, K. Ploog, and R. Merlin, Phys. Rev. Lett. **69**, 973 (1992).

[6] O. Krebs and P. Voisin, Phys. Rev. Lett. **77**, 1829 (1996).

[7] O. Krebs, D. Rondi, J. L. Gentner, L. Goldstein, and P. Voisin, Phys. Rev. Lett. **80**, 5770 (1998).

[8] A. V. Platonov *et al.,* Phys. Rev. Lett. **83**, 3546 (1999).

[9] E. L. Ivchenko, A. Yu. Kamonskii, and U. Rössler, Phys. Rev. B **54**, 5852 (1996).

[10] H. Im, P. C. Klipstein, R. Grey, and G. Hill, Phys. Rev. Lett. **83**, 3693 (1999).

[11] L. A. Cury, D. K. Maude, F. Aristone, J. C. Portal, D. L. Sivco, A. Y. Cho, and G. Hill, Surf. Sci. **267**, 383 (1992).

[12] R. K. Hayden *et al.,* Phys. Rev. Lett. **66**, 1749 (1991).

[13] T. B. Boykin, R. E. Carnahan, and K. P. Martin, Phys. Rev. B **50**, 15 393 (1994). Boykin *et al.* define a parameter λ, requiring $\lambda^2 \ll 1$. In our case $\lambda \approx 0.5$.

[14] A. Zaslavsky, Yuan P. Li, D. C. Tsui, M. Santos, and M. Shayegan, Phys. Rev. B **42**, 1374 (1990).

[15] P. C. Klipstein, in the *24th International Conference on the Physics of Semiconductors, 1998,* edited by M. Heiblum and E. Cohen (World Scientific, Singapore, 1999); CD-ROM file: 1265.pdf (1999); we note that the integration length for the matrix elements in Eq. (1) of Ref. [15] may be $a_0/2$ because of the quasiperiodic nature of the bulk microscopic crystal potential, where $V_I(x, y, z) = V_I(x, y - a_0/2, z + a_0/2)$. In this case it is easy to show that the square bracket in that equation has zero contribution from the Γ_{15} bands, which are nearest in energy, and negligible contribution from all other bands, which are remote. The treatment in Ref. [15] then works with $L = a_0/2$, i.e., the range of the interface potential is $\sim \pm a_0/4$, consistent with the range adopted in Ref. [16]. In fact, the effective mass and band edge at an abrupt interface, such as *AI* or *IB* of Ref. [15], do not change abruptly as stated there, but also over a range $\sim \pm a_0/4$. This does not affect the treatment significantly.

[16] B. A. Foreman, Phys. Rev. Lett. **81**, 425 (1998).

[17] G. Bastard, *Wave Mech. applied to Semicond. Het.* (Halstead Press, NY, 1988).